# Optimal harmonic response in a confined Bödewadt boundary layer flow

Younghae Do
*Department of Mathematics, Kyungpook National University, Daegu 702-701, Korea*

Juan M. Lopez*
*School of Mathematical and Statistical Sciences, Arizona State University, Tempe, Arizona 85287, USA*

Francisco Marques
*Departament de Física Aplicada, Universitat Politècnica de Catalunya, 08034 Barcelona, Spain*

(Received 17 May 2010; published 1 September 2010)

The Bödewadt boundary layer flow on the stationary bottom end wall of a finite rotating cylinder is very sensitive to perturbations and noise. Axisymmetric radial waves propagating inward have been observed experimentally and numerically before the appearance of spiral three-dimensional instabilities. In this study, the sensitivity and response of the finite Bödewadt flow to a harmonic modulation of the rotation rate are analyzed. A comprehensive exploration of response to variations in the amplitude and frequency of the forcing has been carried out. There are sharply delineated linear- and nonlinear-response regimes, with a sharp transition between them at moderate amplitudes. The periodic forcing leads to a steady-streaming flow, even in the linear-response regime, and to a period-doubling bifurcation in the nonlinear regime. Frequency response curves at different forcing amplitudes over a wide range of frequencies have been computed and used to identify the frequency band that excites the axisymmetric radial waves and the forcing frequency that elicits the strongest response. Finally, we have shown that the axisymmetric waves always decay to the steady basic state when the harmonic modulation is suppressed, and conclude that the experimentally observed persistent circular waves are not self-sustained.

DOI: 10.1103/PhysRevE.82.036301 PACS number(s): 47.20.Ib, 47.20.Ky, 05.45.−a

## I. INTRODUCTION

The Bödewadt boundary layer is the boundary layer that forms on a stationary flat surface when the flow aloft rotates. Bödewadt [1] found an analytical description for an idealized situation of unbounded rotating flow above a horizontally infinite plane by implementing techniques used earlier by von Kármán [2] for the self-similar flow above a rotating disk of infinite radius. These flows are of fundamental interest, and variants of them appear in many diverse contexts, such as geophysical boundary layer flows, turbomachinery, and also as prototypical cross flows in aerodynamic applications; they have been the subject of numerous reviews [3–9]. Yet the Bödewadt boundary layer remains an enigma.

Experiments designed to investigate its stability and the transition to turbulence in such flows are by physical necessity conducted using flows of finite extent, and in order to reduce the effects of extraneous noise, they are typically conducted using enclosed flows. When the flow aloft the stationary bottom boundary is in slow rotation, the vertical profiles of the boundary layer up to about 80% of the radial distance from the rotation axis to the enclosure wall are very well described by the similarity solution of Bödewadt [1]. As the rotation rate is increased, experiments typically report the appearance of a train of axisymmetric waves at roughly 50% radius that propagate radially inward with nonuniform speed [10–17]. These axisymmetric waves also appear as transients at slower rotation rates when the rotation rate is changed even only slightly, both when the change is impulsive and when it is smooth. In spite of these observations, linear stability analysis and nonlinear simulations at rotation rates corresponding to those of the experiments show that these axisymmetric waves are transients, and that the flow only becomes unstable at yet higher rotation rates to multiarmed spirals [18], which are also observed in many of the above cited experiments at the higher rotation rates.

States that are linearly stable to perturbations but manifest instability in experiments in the same neighborhood of parameter space are well known: plane Couette flow, Poiseuille flow, the wake of a backward facing step, etc. These are all open flows, and so the concepts of convective and absolute instability are often applied to explain the observed unstable flow [19,20]. In contrast, the finite Bödewadt flow and other rotor-stator flows are completely enclosed flows. It has been suggested that even in enclosed flows, a local variant of the concept of convective instability may be applicable [9]. Also, for all these flows, the perturbation eigenmodes are not orthogonal and so the concepts of transient growth have also been suggested as playing a role in the growth of instabilities [21–23]. Both the local convective instability and the transient growth due to non-normality are linear processes that are formulated using a linearization about the basic state where no account is taken of mean-flow distortions.

The axisymmetric waves observed experimentally in the finite Bödewadt flow are either a response to impulsive or harmonic perturbations to the basic state that are on the order of a few percent of the magnitude of the base flow; at first glance, these levels of perturbation may seem to be small enough to be considered within the linear regime. The continuous presence of extraneous noise above a threshold level

*lopez@math.asu.edu

 

in experiments has also been reported to sustain these axisymmetric waves (experiments conducted with a noisy motor leads to waves, but when the motor is replaced with a quieter one the waves are not present in the same parameter regime [16]). The noise levels involved in the experiments are also only on the order of a few percent of the magnitude of the base flow.

In this paper, we explore numerically the finite Bödewadt flow by subjecting it to harmonic forcing with amplitudes down to very low levels, of order $10^{-3}$% of the base flow, and have found a sharp cutoff between an essentially linear-response regime and a nonlinear-response regime which is manifest at forcing levels of about 0.5%. In the linear-response regime, the amplitude of the response axisymmetric wave modes is proportional to the forcing amplitude, whereas in the nonlinear regime the magnitude of the response waves, relative to the magnitude of the forcing, diminishes with forcing amplitude (but the overall response amplitude still grows with forcing amplitude). In the nonlinear regime, there are strong nonlinear interactions between the response flow and the base flow, and this is manifest in nontrivial time averages, the so-called nonlinear steady-streaming flow [24,25]. Furthermore, the linear regime is well characterized by an optimal forcing frequency that is independent of the forcing amplitude, whereas in the nonlinear regime, the optimal frequency shifts considerably for increasing forcing amplitudes, very likely due to mean-flow modifications. It is only by subtracting the base state from the response flow in our simulations that we have been able to detect the response waves at the low forcing amplitudes of the linear regime. Very likely, if the experiments are able to do same they will also observe the linear-response waves. However, harmonically forced experiments have typically been conducted in what we find to be the nonlinear-response regime; for example, Gauthier *et al.* [16] use a forcing amplitude of 6.5%

We also show that stopping the harmonic forcing after the synchronized state with circular waves has been fully established results in the flow quickly reverting back to the basic steady state. This happens within about ten forcing periods after the forcing has ceased. For these problems, the transient time for the establishment of the wave-train synchronized state, even from another synchronized state at a slightly different forcing amplitude and frequency, is about 300 forcing periods. This reversion to the basic state is true even for the synchronized states with the largest forcing amplitudes at the optimal forcing frequencies. This clearly demonstrates that the circular wave state is not self-sustained.

## II. GOVERNING EQUATIONS AND NUMERICAL METHODS

Consider the flow in a circular cylinder of height-to-radius aspect ratio $\gamma=H/R$, completely filled with a fluid of kinematic viscosity $\nu$. The cylinder and the top end wall rotate with angular speed $\Omega(t)=\Omega_0(1+\alpha \sin \omega t)$ while the bottom end wall is stationary; the nondimensional parameters $\alpha$ and $\omega$ are the amplitude and frequency of the modulated rotation. A schematic of the flow system is shown in Fig. 1. The

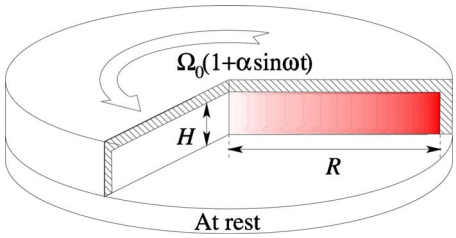


FIG. 1. (Color online) Schematic of the finite Bödewadt flow. The inset shows the vortex lines (contours of $rv$) of the flow for $\mathrm{Re}=5\times10^4$ and $\gamma=0.2$, with $\alpha=0$, at steady state.

Navier-Stokes equations, nondimensionalized using the radius $R$ as the length scale and the mean rotation rate to set the time scale $1/\Omega_0$, are

$$(\partial_t + \mathbf{u}\cdot\nabla)\mathbf{u} = -\nabla p + \frac{1}{\mathrm{Re}}\nabla^2\mathbf{u}, \quad \nabla\cdot\mathbf{u}=0, \tag{1}$$

where $\mathbf{u}=(u,v,w)$ is the velocity field in polar coordinates $(r,\theta,z)\in[0,1]\times[0,2\pi]\times[0,\gamma]$ and $p$ is the kinematic pressure. The problem has four independent nondimensional parameters: the Reynolds number $\mathrm{Re}=\Omega_0R^2/\nu$, the radius-to-height aspect ratio $\gamma$, and the amplitude and frequency of the modulated rotation $\alpha$ and $\omega$. In the earlier study [18], the modulated problem was only considered at fixed modulation amplitude $\alpha=0.05$ (which as we shall see is quite large and leads to significant mean-flow modifications) and fixed modulation frequency $\omega=1.0$, which is too small to capture the most aggressively driven circular waves at the smaller amplitudes considered here. We consider $\alpha\in(10^{-6},0.05)$ and a wide range of frequencies $\omega\in(0.5,5.0)$, covering the region where the response to the forcing is significant.

The boundary conditions are no slip: on the rotating cylinder sidewall $(u,v,w)=(0,1+\alpha\sin\omega t,0)$, on the rotating top end wall $(u,v,w)=(0,r[1+\alpha\sin\omega t],0)$, and on the bottom stationary end wall $(u,v,w)=(0,0,0)$. The idealized boundary conditions are discontinuous at the junctions where the rotating cylinder meets the stationary bottom end wall at $(r=1,\ z=0)$. In a physical experiment there is a small but finite gap at this junction where the azimuthal velocity adjusts rapidly to zero. For an accurate use of spectral techniques, a regularization of this discontinuity is implemented of the form

$$v(r,\theta,0,t)=(1+\alpha\sin\omega t)\exp\left(\frac{r-1}{\epsilon}\right), \tag{2}$$

where $\epsilon$ is a small parameter that mimics the small physical gaps (we have used $\epsilon=0.003$). The use of $\epsilon\neq0$ regularizes the otherwise discontinuous boundary condition; see Ref. [26] for further details on the use of this technique in spectral codes.

The governing equations (1) have been solved using a second-order time-splitting method, with space discretized via a Galerkin-Fourier expansion in $\theta$ and Chebyshev collocation in $r$ and $z$. The spectral solver is based on that described in Ref. [27], and it has recently been tested and used on this problem [18]. For the solutions presented here, with $\gamma=0.2$, we have used $n_r\times n_z=96\times48$ Chebyshev modes in

FIG. 2. (Color online) Contours of azimuthal vorticity $\eta$ for the steady basic state at $\mathrm{Re}=5\times10^4$ and $\gamma=0.2$ using $n_r\times n_z=96\times48$ and $\delta t=5\times10^{-3}$; the contours are in the range $\eta\in[-5,5]$.

the radial and axial directions; since we are concerned with the circular waves in this paper, all the simulations have been restricted to the axisymmetric subspace. Time steps of the order $\delta t=10^{-3}$ have been required for numerical stability and accuracy of the second-order temporal scheme. Typically, we have used 1000 time steps per forcing period; however, for very low forcing frequencies, more time steps per period are required in order to maintain $\delta t\leq10^{-3}$.

## III. BASIC STATE AND ITS STABILITY

The basic state has been extensively described and discussed previously [12,13,28], and its linear stability to general three-dimensional perturbations has recently been determined [18], and so only a brief overview is presented here. For any aspect ratio $\gamma$, if Re is large enough the boundary layers on the disks are separated by an interior region which is nominally rotating with a near solid-body rotation distribution of angular momentum, except close to the cylinder sidewall. However, it is never exactly solid-body rotation as the flow in the top disk boundary layer is centrifuged radially outward while that in the bottom disk boundary layer is drawn radially inward. Over a considerable radial extent (about 80%), the radial velocity in the interior is very small and the angular momentum distribution is almost $z$ independent, but does not correspond to solid-body rotation. Figure 2 shows the azimuthal component of vorticity $\eta=\partial u/\partial z-\partial w/\partial r$ for the steady axisymmetric basic state at $\mathrm{Re}=5\times10^4$ and $\gamma=0.2$. The figure clearly shows the boundary layers on the top, bottom, and sidewall. While the boundary layer thickness along the top rotating disk is quite uniform, the boundary layer thickness on the bottom stationary disk varies considerably with $r$, thickening as $r$ is reduced. The sidewall layer also shows considerable variation with $z$. It has been well established that the boundary layer on the bottom has the characteristic oscillatory vertical structure of the Bödewadt solution with the expected $\mathrm{Re}^{-1/2}$ scaling of its thickness over a wide range of Re's [13,18,28]. The thickening of the Bödewadt layer with decreasing $r$ and the $\mathrm{Re}^{-1/2}$ scaling of the thickness have also been observed in experiments in a much shallower rotor-stator system with $\gamma=0.05$ [16], where the nonparallel nature of the boundary layer on the stationary disk was also noted.

The linear stability of the basic state to general three-dimensional perturbations was determined using global linear stability analysis via time evolution of the Navier-Stokes equations [18]. First, a steady axisymmetric basic state was computed at some point in parameter space. Its stability was determined by introducing small random perturbations into all azimuthal Fourier modes. For sufficiently small perturbations, the nonlinear couplings between Fourier modes are negligible (below round-off numerical noise) and the growth rates (real parts of the eigenvalues) and structure of the eigenfunctions corresponding to the fastest growing perturbation at each Fourier mode emerge from time evolution. This is tantamount to a matrix-free generalized power method in which the actions of the Jacobian matrices for the perturbations are given by time integration of the Navier-Stokes equations with the aforementioned initial conditions.

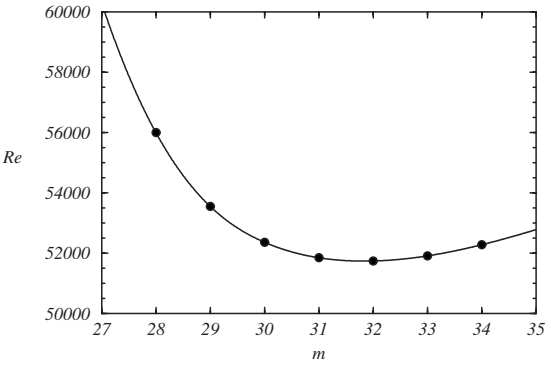


FIG. 3. Marginal stability curve for $\gamma=0.2$ showing the critical Re at which the axisymmetric basic state loses stability via supercritical Hopf bifurcations to spiral rotating waves with azimuthal wave number $m$. The lines connecting the symbols are a guide for the eye as the wave numbers $m$ are integers.

For $\gamma=0.2$, the critical Re's for the most dangerous Fourier modes are plotted in Fig. 3. The basic state first loses stability at $\mathrm{Re}_c=51\,743$ to an $m=32$ spiral rotating wave. The extensive stability analysis conducted by Lopez *et al.* [18] established that the steady basic state is linearly stable with respect to axisymmetric perturbations ($m=0$), at least up to the highest Re considered, $\mathrm{Re}=10^5$. However, for $\mathrm{Re}>10^3$ transient circular waves exist in the stationary disk boundary layer.

## IV. RESPONSE TO HARMONIC MODULATION

We now consider the response of the basic state to harmonic modulation of the rotation of the cylinder top and sidewall, for a mean Reynolds number $\mathrm{Re}=5\times10^4$, below but close to the critical value $\mathrm{Re}_c$. We consider a wide range of amplitudes, $\alpha\in[10^{-5},0.05]$. The largest amplitude means that the instantaneous Re reaches $5.25\times10^4$, which is a little above critical for the onset of the $m=32$ spiral mode. However, it is at this level for only a very short time during part of the forcing period, too short for the spirals to saturate nonlinearly, and during most of the forcing period, the nonaxisymmetric perturbations are damped. For $\alpha<0.035$, nonaxisymmetric perturbations are damped during the whole forcing period, and the vast majority of the results presented in this paper are in this regime. We have considered frequencies in the range $\omega\in[0.5,5.0]$; the largest responses to harmonic forcing are for $\omega\in[1.5,3.0]$. The earlier study [18] only considered $\omega=1.0$, and so missed much of the phenomena associated with the optimal response regime.

Figure 4 shows snapshots of the azimuthal vorticity $\eta$ that results from subjecting the basic state at $\mathrm{Re}=5.0\times10^4$,

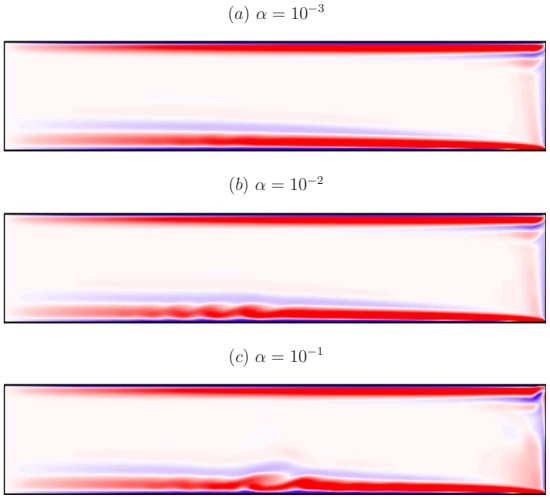


FIG. 4. (Color online) Snapshots of the azimuthal vorticity $\eta$ at $\mathrm{Re}=5\times10^4$, $\gamma=0.2$, $\omega=2.2$, and $\alpha$ as indicated. The color-map levels are such that $\eta\in[-5.0,5.0]$ with blue (light) being negative and red (dark) being positive (see associated movies [41]).

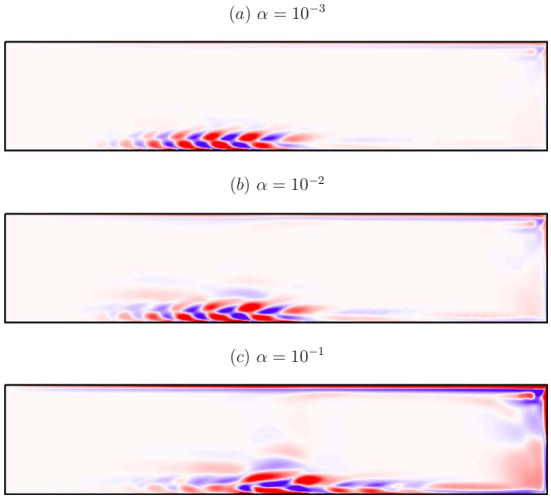


FIG. 5. (Color online) Snapshots of $\eta(t)-\eta_o$, at $\mathrm{Re}=5\times10^4$, $\gamma=0.2$, $\omega=2.2$, and $\alpha$ as indicated. The color-map levels are such that $\eta(t)-\eta_o\in[-0.2,0.2]$ for $\alpha=10^{-3}$, $\eta(t)-\eta_o\in[-1.0,1.0]$ for $\alpha=10^{-2}$, and $\eta(t)-\eta_o\in[-2.0,2.0]$ for $\alpha=10^{-1}$, with blue (light) being negative and red (dark) being positive (see associated movies [41]).

shown in Fig. 2, to harmonic forcing at $\alpha=10^{-3}$, $10^{-2}$, and $10^{-1}$, all with forcing frequency $\omega=2.2$. These are taken after about 300 forcing periods, the time needed for transients to decay and the system to settle into a periodic state synchronous with the forcing. In the $\alpha=10^{-3}$ case, there is hardly any evidence of the harmonic forcing, and the state is almost indistinguishable from the basic state; however, viewing the associated online movie [41] shows that there are some very slight variations in the bottom boundary layer for $r\in(0.4,0.5)$. Increasing the amplitude to $\alpha=10^{-2}$ results in a periodic wave train that first becomes evident at about $r=0.5$ in the bottom boundary and propagates toward $r=0$. As they propagate radially inward, they slow down and fade out by about $r=0.25$. Apart from the bottom boundary layer region for $r\in(0.25,0.40)$, the rest of the flow appears stationary and virtually identical to the basic state. Increasing the amplitude further to $\alpha=10^{-1}$ leads to a significant response throughout the entire cylinder. The largest response is still concentrated in the bottom boundary layer region for $r\in(0.25,0.40)$ where a periodic train of waves propagating radially inward is present. These are more intense than at the lower $\alpha$, but still slow down and fade out as they approach $r\approx0.25$. Now, there is also a strong response in the corner region, $(r,z)=(1,0.2)$, as well as in the sidewall boundary layer, which show large pulses of $\eta$ with alternating sign propagating down the sidewall as they emanate from the corner. These pulses appear to be absorbed into the bottom corner region, $(r,z)=(1,0)$.

Clearly, for the larger $\alpha$, the forcing is not only triggering a wave train in the bottom boundary, but it is also modifying the base flow, whereas for the low $\alpha$, the response is so weak compared to the base flow that it is difficult to appreciate any response. However, subtracting the base flow from the response flow, denoted as $\eta(t)-\eta_o$, gives us a very good indication of the nature of the response flow. Figure 5 shows contours of $\eta(t)-\eta_o$ for the three cases shown in Fig. 4, and the accompanying movies with the online version of the paper shows their evolution over one forcing period [41]. For the smaller forcing amplitudes, we see that there is in fact a wave-train response in the bottom boundary layer, but that its magnitude is swamped by the mean flow. We also see that there is a response in the top corner, but that this is very much weaker than the circular waves. As the forcing amplitude is increased, the strength of the response in the top and sidewall boundary layers, and the top corner where they meet, becomes stronger relative to the wave-train response in the bottom boundary layer. The top boundary layer response shows the expected sheets of oppositely signed vorticity traveling normal to the boundary layer and quickly fading away. This behavior is of the form considered by Yih's [29] analysis of the boundary layer on a rotating infinite disk subjected to harmonic modulation of the rotation. We have previously simulated the flow in a rotating cylinder where the whole cylinder is modulated [30] and have found very good agreement between the computed boundary layer structure and Yih's theory.

In order to quantify the response of the Bödewadt layer to harmonic forcing, we consider the maximum of $\eta(t)-\eta_o$ over the region $(r,z)\in[0,0.8]\times[0,0.1]$ and over one forcing period; this excludes the top and sidewall boundary layers, which can dominate for some combinations of $\alpha$ and $\omega$ [see Fig. 5(c)]. We determined the maximum over two forcing periods, for as is discussed later, for larger $\alpha$ values the response is not synchronous with the forcing but instead has a period twice that of the forcing. The results are summarized in Fig. 6. The response $\max[\eta(t)-\eta_o]$ corresponds to the most intense contribution from the circular waves in the bottom boundary, as seen in the movies associated with Fig. 5 [41]. We have considered many values of $\alpha$; the plots show only a few cases for the sake of clarity of presentation. For $\alpha\lesssim4\times10^{-3}$, $\max[\eta(t)-\eta_o]$ scales linearly with $\alpha$ across all $\omega$. This linear scaling is borne out by the excellent collapse of $\max[\eta(t)-\eta_o]$ for these small $\alpha$ of the curves in Fig. 6(a). For larger $\alpha$ the linear scaling is lost and the response at a

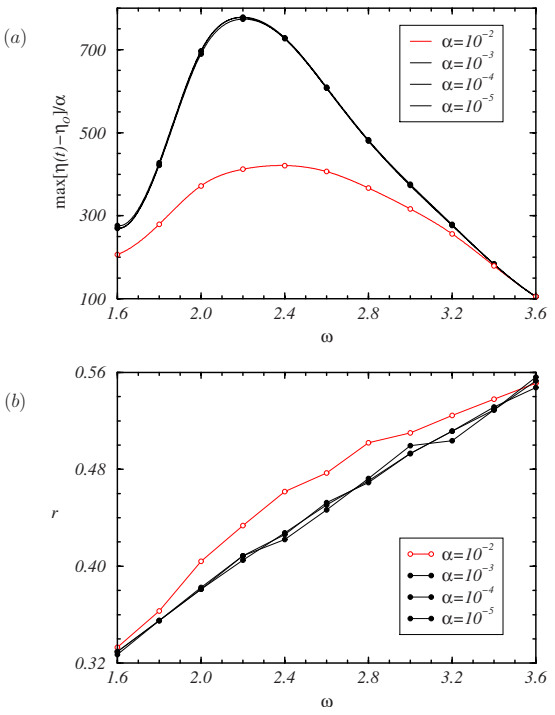


FIG. 6. (Color online) Frequency response curves for several forcing amplitudes $\alpha$ as indicated; (a) shows the response magnitude as measured by $\max[\eta(t)-\eta_o]$, where the maximum is determined over $r\in[0,0.8]\times z\in[0,\gamma]$ and $t\in[2n\pi/\omega,2(n+1)\pi/\omega]$, with $n$ sufficiently large for transients to have died out, and (b) shows the radial location of the maxima in (a).

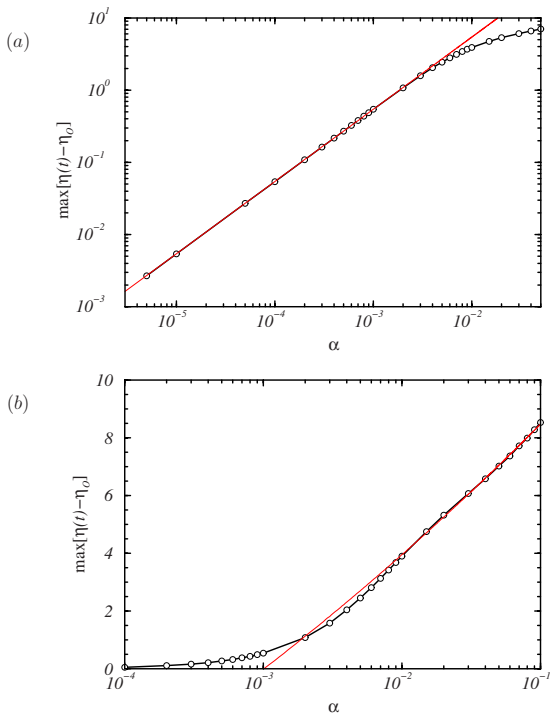


FIG. 7. (Color online) Maximal responses $\max[\eta(t)-\eta_o]$ versus $\alpha$ for $\omega=2.2$. The red (light) lines are curve fits for low and high $\alpha$ values: (a) $\max[\eta(t)-\eta_o]=779\alpha$ and (b) $\max[\eta(t)-\eta_o]=-28.7+42.3\alpha^{0.056}$.

given $\alpha$ varies with $\omega$. The strongest response for small $\alpha$ is at $\omega\approx 2.2$. For small $\omega\lesssim 0.5$ and for large $\omega\gtrsim 5.0$, there are no circular waves evident in the bottom boundary, even for the larger $\alpha$ values considered. The radial location of where the circular waves attain maximum strength is summarized in Fig. 6(b); again for $\alpha\lesssim 4\times 10^{-3}$ we find self-similar behavior, and for all $\alpha$ the radial location where the waves are most intense shifts from $r\approx 0.32$ to $r\approx 0.56$ as $\omega$ is increased.

For forcing frequency $\omega=2.2$, which for $\alpha\lesssim 0.004$ is optimal in generating the circular wave train, we present in Fig. 7 the maximum of $\eta(t)-\eta_o$ over two forcing periods in the bottom boundary layer. The results are shown in two plots. In Fig. 7(a), we use a log-log plot and fit a straight line to the small-$\alpha$ data, given by $\max[\eta(t)-\eta_o]=779\alpha$. This plot further quantifies the $\alpha$ extent over which the wave-train magnitude scales linearly with $\alpha$ (up to $\alpha\approx 0.004$). For larger $\alpha$, Fig. 7(b) shows a power-law scaling of the form $\max[\eta(t)-\eta_o]=-28.7+42.3\alpha^{0.056}$. This scaling provides a very good fit to the data for $\alpha\in(0.008,0.1)$. These plots clearly show the two response regimes and the sharp transition between them occurring for $\alpha\in(0.004,0.008)$. For $\alpha>0.1$, the mean-flow modifications, particularly near the sidewall, are very large and the problem becomes very different from the one we wish to study.

### A. Steady-streaming flow

The mean-flow modifications that result due to the larger amplitude harmonic modulations are typical in periodically forced flows. In these oscillating flows, Reynolds stress terms appear in the time-averaged Navier-Stokes equations that lead to a steady secondary motion known as steady streaming, first discovered by Schlichting [31]. The strength of the steady-streaming flow depends on the amplitude and frequency of the oscillations as well as the nature of the base flow in the absence of oscillations. While there have been numerous studies of steady-streaming flows due to oscillations about a static base, there are relatively few studies with strong base flows [30,32–35]. Figure 8 shows the steady-streaming flow for the cases shown in Fig. 5, computed by taking the time average over two forcing periods $\langle\eta(t)-\eta_o\rangle=(\omega/4\pi)\int_0^{4\pi/\omega}\eta(t)dt-\eta_o$. We see that even though the instantaneous response is primarily in the form of the wave train in the bottom boundary layer, the time average extends considerably into the interior and also has a considerable presence in the top boundary layer, even for the low-$\alpha$ cases. Large time-averaged flows imply significant mean-flow modification as a result of the imposed modulation. Note that all linear theories (transient growth and local stability analysis) assume no mean-flow modification, and so these nontrivial steady-streaming flows call into question the limitations of the applicability of the linear analyses.

To provide a quantitative measure of the strength of the steady-streaming flow, we plot in Fig. 9 the maximum of the time-averaged relative vorticity, $\max\langle\eta(t)-\eta_o\rangle$, in the Bödewadt layer versus $\alpha$ for $\omega=2.2$. The plot shows two distinct regimes, as did the instantaneous measure in Fig. 7. In the low-$\alpha$ regime, the magnitude of the steady-streaming flow scales like $\alpha^2$ while the instantaneous flow scaled linearly with $\alpha$. This means that while the magnitude of the

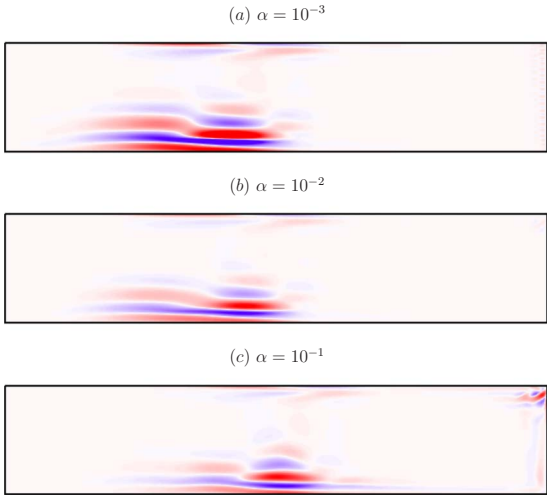


FIG. 8. (Color online) Time-averaged perturbation azimuthal vorticity, $\langle \eta(t) - \eta_o \rangle$, at Re$=5\times10^4$, $\gamma=0.2$, $\omega=2.2$, and $\alpha$ as indicated. For the $\alpha=10^{-3}$ case, the color map has $\min/\max\langle \eta(t)-\eta\rangle = \mp 0.001$, for $\alpha=10^{-2}$ the color map has $\min/\max\langle \eta(t)-\eta\rangle = \mp 0.05$, and for $\alpha=0.1$ the color map has $\min/\max\langle \eta(t)-\eta\rangle = \mp 0.2$; red (dark) is positive and blue (light) is negative.

circular waves decreases linearly to zero with $\alpha$, their time average and hence their impact on the background flow diminish to zero quadratically with $\alpha$, i.e., it is a nonlinear effect. In the high-$\alpha$ regime, however, the growth of the magnitude of the circular waves with increasing $\alpha$ is very slow, scaling like $\alpha^{0.056}$, whereas the steady-streaming flow in this regime grows considerably faster, scaling like $\alpha^{0.455}$. This rapidly results in the steady-streaming flow causing considerable modifications to the base state being modulated. The transition to this highly nonlinear regime occurs for what one would regard as quite small forcing amplitudes of around 0.5%, and this is about an order of magnitude smaller than the forcing amplitudes typically used in experiments [16].

### B. Period-doubled regime

In the nonlinear regime, with $\alpha \gtrsim 0.004$, we have found that the synchronous state loses stability via a period-doubling bifurcation. Figure 10 shows the period-doubling bifurcation curve in the $(\omega,\alpha)$-parameter space for Re$=5\times10^4$ and $\gamma=0.2$. The bifurcation point emerges very broadly in $\omega$ from a point at about $(\omega,\alpha)=(2.8,0.005)$. Figure 11 shows space-time plots of two typical states in the nonlinear regime. Figure 11(a) is for a synchronous state at $\alpha=0.01$ and $\omega=2.2$ and Fig. 11(b) is for a period-doubled state at $\alpha=0.01$ and $\omega=2.7$. They both show color-map contours of $\eta(t)-\eta_o$ at a height $z=0.01$, which is in the Bödewadt layer; the vertical direction is $r$, from the sidewall at $r=1$ at the bottom to the axis at $r=0$ at the top. The horizontal direction is time; both show a time interval of about 86 time units, which for the $\omega=2.2$ case corresponds to 30 forcing cycles and for $\omega=2.7$ it corresponds to 37 forcing cycles. In the synchronous case, we see a weak disturbance that propagates radially inward from the sidewall at a fairly uniform speed until it reaches $r\approx0.5$ where it suddenly slows down and is amplified [this is where the circular waves become visible, for example, in the movie associated with Fig. 4(b)]. The waves continue propagating radially inward, slowing down slightly, and fading away by the time they reach $r\approx0.2$. Increasing $\omega$ to 2.7, we cross the period-doubling bifurcation curve. The resulting period-doubled

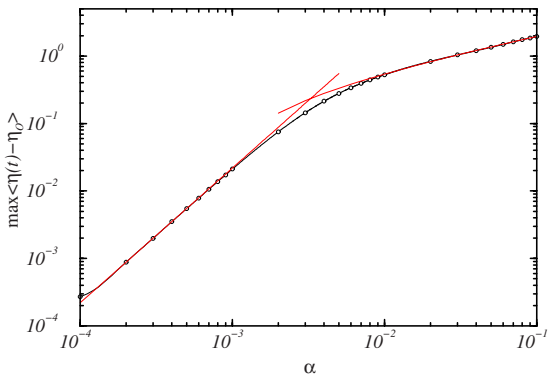


FIG. 9. (Color online) Maximum of the time-averaged relative vorticity, $\max\langle \eta(t)-\eta_o\rangle$, in the Bödewadt layer versus $\alpha$ for $\omega=2.2$. The two curve fits are $\max\langle \eta(t)-\eta_o\rangle = 2.2\times10^4\alpha^2$ in the low-$\alpha$ regime and $\max\langle \eta(t)-\eta_o\rangle = 6.2\alpha^{0.455}-0.224$ in the high-$\alpha$ regime.

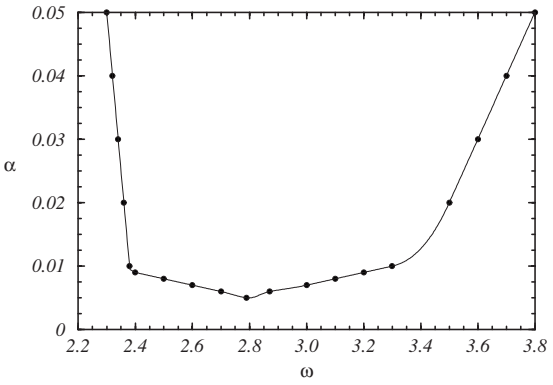


FIG. 10. Period-doubling bifurcation curve in $(\omega,\alpha)$-parameter space for Re$=5\times10^4$ and $\gamma=0.2$; below the curve the synchronous state is stable.

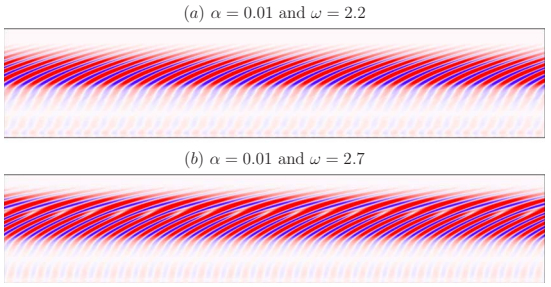


FIG. 11. (Color online) Space-time plots of $\eta(t)-\eta_o$ at $z=0.01$ (in the Bödewadt boundary layer) at Re$=5\times10^4$ and $\gamma=0.2$ for (a) the synchronous state at $\alpha=0.01$ and $\omega=2.2$, and (b) the period-doubled state at $\alpha=0.01$ and $\omega=2.7$. The color maps are in the range $\eta(t)-\eta_o\in[-1,1]$ with blue (light) being negative and red (dark) being positive. The vertical axis is the radial direction from $r=1$ (bottom) to the axis $r=0$ (top), and the horizontal axis is time showing 30 forcing periods for the $\omega=2.2$ case and 37 forcing periods for the $\omega=2.7$ case.

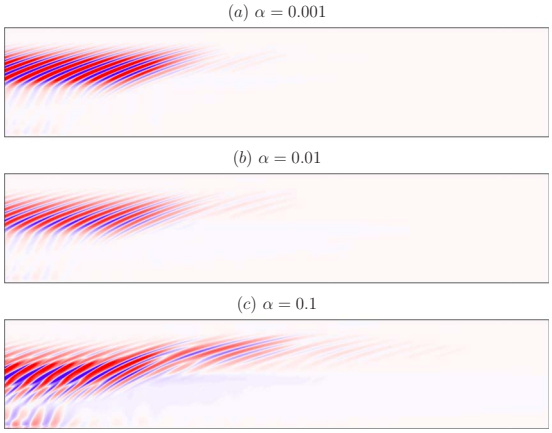


FIG. 12. (Color online) Space-time plots of $\eta(t)-\eta_0$ in the Bödewadt layer at height $z=0.01$ (vertical axis $r$ from the sidewall $r=1$ at the bottom to $r=0$ at the top, and the horizontal axis is time, with $t=0$ at the left when the harmonic forcing is instantaneously set to zero, to $t=86$), all for $\mathrm{Re}=5\times10^4$, $\gamma=0.2$, $\omega=2.2$, and $\alpha$ of the initial oscillatory state as indicated.

state behaves much like the synchronous state, except that the waves are a little more intense and the initial disturbance at large $r$ slows down at a larger $r$. The resulting circular waves now propagate with a more nonuniform speed than in the synchronous case, decelerating more. The combination of more intense (and hence larger) waves and a greater deceleration results in the collision and merger between a decelerating wave and a faster moving wave behind it. The wave coming from behind merges into the leading wave, and so the next wave does not catch the merged wave, but the next wave to follow catches and merges with it, and so the whole process repeats itself, once every two forcing periods.

These types of collision and merger events of circular waves in Bödewadt boundary layers were first observed and described by Lopez and Weidman [12] who found them in both physical experiments and numerical simulations of the impulsive spin down to the rest of the flow in a rotating circular cylinder. They have subsequently also been observed in rotor-stator experiments with a stationary cylindrical shroud [14,15,17].

### C. Switching off the forcing

After obtaining a synchronous (or period-doubled) state with circular waves, if we turn off the harmonic forcing the flow continues to stay close to the ghost of the synchronous state for several wave cycles, but always decays to the steady basic state. Figure 12 shows some typical examples; these are space-time plot like those in Fig. 11. The initial conditions in these are the synchronous states at $\omega=2.2$ with $\alpha=0.1$, 0.01, and 0.001. So what does this mean? These simulations suggest that there is no wave state disconnected from the basic state that is reached due to transient growth (i.e., non-normal growth of an optimal perturbation applied instantaneously at some point in time and allowed to grow). We only have sustained waves when the systems are continuously subjected to external forcing.

Nonmodal instability theories, e.g., [36], suggest that even small external perturbations may undergo a strong transient amplification and trigger nonlinear dynamics. When external perturbations are switched off, such an externally forced perturbed state would decay in the long term according to linear theory, but can survive forever due to nonlinear interactions if finite amplitudes are reached. Such theories lead to the concept of an "elephant mode" [37], a naturally selected finite-amplitude self-sustained mode. Recent direct numerical simulations of the flow between two corotating disks with radial throughflow [38] have reported the existence of such a mode.

In the simulations presented here, regardless of whether we drive the system in the linear ($\alpha<0.004$) or nonlinear ($\alpha>0.004$) regime, if we turn off the harmonic forcing after the nonlinear synchronous state with circular waves is fully developed, the flow always reverts to the steady basic state after a short transient (the equivalent of about a dozen forcing cycles). This implies that the experimentally observed persistent circular wave trains are not a self-sustained elephant mode, but rather are noise sustained, and the boundary layer selectively amplifies wave trains with a limited band of frequencies (so-called amplifier dynamics [39]).

## V. CONCLUSIONS

Subjecting the finite Bödewadt boundary layer to harmonic forcing has revealed several interesting insights. The boundary layer on the stationary bottom end wall is driven by the rotation of the enclosing top and sidewall of a finite cylinder, and the harmonic forcing consists of a small amplitude modulation of the rotation. In parameter regimes where the unforced system is steady and axisymmetric, the harmonic forcing produces periodic axisymmetric wave trains in the Bödewadt boundary layer. By considering a wide range of forcing frequencies and forcing amplitudes ranging from about 10% of the background rotation to amplitudes many orders of magnitude smaller, we have identified two distinct regimes. One is the linear-response regime where the magnitude of the circular waves is linearly proportional to the forcing amplitude. The other is the nonlinear-response regime, where the circular wave amplitudes have a power-law scaling with forcing amplitude and, instead of being synchronized with the forcing, undergo a period-doubling bifurcation over a large range of parameter space in this regime.

There is a well-defined forcing frequency at which the circular wave train is of maximal strength, and in the linear-response regime this optimal forcing frequency is independent of the forcing amplitude. At first sight, this may suggest a resonance-type behavior: a possible explanation of the frequency response curve and the optimal forcing frequency at which the response reaches the maximum value could be a 1:1 resonance with a Hopf eigenvalue of the base state before it bifurcates, and therefore the Hopf mode is still unstable. However, since it is close to the bifurcation point, the Hopf mode becomes excited when forced precisely at its Hopf frequency [40]. However, in the present problem we have tested up to $\mathrm{Re}=10^5$ and have not found any axisymmetric Hopf eigenmode that bifurcates. Moreover, the resonantly

excited Hopf mechanism just described typically results in response curves with very narrow spikes, while in the present problem the response curve is very broad. Therefore, we must conclude that the circular waves are not related to a global Hopf eigenmode, but rather they are closely associated with the extreme sensitivity of the inflectional Bödewadt boundary layer profile, and this sensitivity is precisely localized in a limited region inside the boundary layer. When the circular waves leave this region, they just fade away, and can only be sustained by the continuous excitation induced by periodic forcing, as in this study, or more generally by noise. The circular waves are thus seen to be a response to mean-flow modifications. The steady-streaming flow driven by the modulations is not negligible even in the linear-response regime, although it scales quadratically with the forcing amplitude and so its influence diminishes rapidly with decreasing forcing amplitude.

## ACKNOWLEDGMENTS

This work was supported in part by the U.S. National Science Foundation Grants No. DMS-0505489 and No. DMS-0922864, the Spanish Ministry of Education and Science Grant No. FIS2009-08821, and the Korean Science and Engineering Foundation WCU Grant No. R32-2009-000-20021-0.

[1] U. T. Bödewadt, Z. Angew. Math. Mech. **20**, 241 (1940).
[2] T. von Kármán, Z. Angew. Math. Mech. **1**, 233 (1921).
[3] A. R. Robinson, Annu. Rev. Fluid Mech. **2**, 293 (1970).
[4] E. R. Benton and A. Clark, Annu. Rev. Fluid Mech. **6**, 257 (1974).
[5] P. J. Zandbergen and D. Dijkstra, Annu. Rev. Fluid Mech. **19**, 465 (1987).
[6] H. Reed and W. Saric, Annu. Rev. Fluid Mech. **21**, 235 (1989).
[7] P. W. Duck and M. R. Foster, Annu. Rev. Fluid Mech. **33**, 231 (2001).
[8] W. S. Saric, H. L. Reed, and E. B. White, Annu. Rev. Fluid Mech. **35**, 413 (2003).
[9] B. Launder, S. Poncet, and E. Serre, Annu. Rev. Fluid Mech. **42**, 229 (2010).
[10] Ö. Savaş, Phys. Fluids **26**, 3445 (1983).
[11] Ö. Savas, J. Fluid Mech. **183**, 77 (1987).
[12] J. M. Lopez and P. D. Weidman, J. Fluid Mech. **326**, 373 (1996).
[13] J. M. Lopez, Phys. Fluids **8**, 2605 (1996).
[14] L. Schouveiler, P. Le Gal, and M. P. Chauve, Phys. Fluids **10**, 2695 (1998).
[15] L. Schouveiler, P. L. Gal, M. P. Chauve, and Y. Takeda, Exp. Fluids **26**, 179 (1999).
[16] G. Gauthier, P. Gondret, and M. Rabaud, J. Fluid Mech. **386**, 105 (1999).
[17] L. Schouveiler, P. Le Gal, and M. P. Chauve, J. Fluid Mech. **443**, 329 (2001).
[18] J. M. Lopez, F. Marques, A. M. Rubio, and M. Avila, Phys. Fluids **21**, 114107 (2009).
[19] P. Huerre and P. A. Monkewitz, Annu. Rev. Fluid Mech. **22**, 473 (1990).
[20] J.-M. Chomaz, Annu. Rev. Fluid Mech. **37**, 357 (2005).
[21] P. J. Schmid and D. S. Henningson, *Stability and Transition in Shear Flows* (Springer, New York, 2001).
[22] P. J. Schmid, Annu. Rev. Fluid Mech. **39**, 129 (2007).
[23] D. Barkley, H. M. Blackburn, and S. J. Sherwin, Int. J. Numer. Methods Fluids **57**, 1435 (2008).
[24] N. Riley, Annu. Rev. Fluid Mech. **33**, 43 (2001).
[25] H. Schlichting and J. Kestin, *Boundary-Layer Theory*, 7th ed. (McGraw-Hill, New York, 1979).
[26] J. M. Lopez and J. Shen, J. Comput. Phys. **139**, 308 (1998).
[27] I. Mercader, O. Batiste, and A. Alonso, Comput. Fluids **39**, 215 (2010).
[28] J. M. Lopez, J. Fluid Mech. **359**, 49 (1998).
[29] C.-S. Yih, *Fluid Mechanics* (West River Press, Ann Arbour, MI, 1977).
[30] A. Rubio, J. M. Lopez, and F. Marques, J. Fluid Mech. **625**, 75 (2009).
[31] H. Schlichting, Phys. Z. **33**, 327 (1932).
[32] C.-Y. Wang, J. Fluid Mech. **41**, 581 (1970).
[33] S. Chawla and A. Verma, Proc. R. Soc. London, Ser. A **386**, 163 (1983).
[34] G. J. Merchant and S. H. Davis, J. Fluid Mech. **198**, 543 (1989).
[35] D. T. Schwartz, Proc. R. Soc. London, Ser. A **442**, 397 (1993).
[36] B. Pier, J. Eng. Math. **57**, 237 (2007).
[37] B. Pier and P. Huerre, J. Fluid Mech. **435**, 145 (2001).
[38] B. Viaud, E. Serre, and J.-M. Chomaz, J. Fluid Mech. **598**, 451 (2008).
[39] O. Marquet, D. Sipp, J.-M. Chomaz, and L. Jacquin, J. Fluid Mech. **605**, 429 (2008).
[40] Y. D. Cui, J. M. Lopez, T. T. Lim, and F. Marques, Phys. Fluids **21**, 034106 (2009).
[41] See supplementary material at http://link.aps.org/supplemental/10.1103/PhysRevE.82.036301 for Document No. X1 for animations of cases a, b, and c over one forcing period.